Two isoleucyl tRNAs that decode 'synonymous' codons divergently regulate breast cancer progression

Lisa B. Earnest-Noble[1], **Dennis Hsu**[1], **Siyu Chen**[2,3,4], **Hosseinali Asgharian**[2,3,4], **Mandayam Nandan**[1], **Maria C. Passarelli**[1], **Hani Goodarzi**[2,3,4,*], **Sohail F. Tavazoie**[1,*]

[1]Laboratory of Systems Cancer Biology, The Rockefeller University, 1230 York Avenue, New York, NY 10065, USA.

[2]Department of Biochemistry and Biophysics, University of California, San Francisco, San Francisco, CA 94158, USA

[3]Department of Urology, University of California, San Francisco, San Francisco, CA 94158, USA

[4]Helen Diller Family Comprehensive Cancer Center, University of California, San Francisco, San Francisco, CA 94158, USA

Abstract

The human genome contains 61 codons that encode for the 20 amino acids. The synonymous codons representing a given amino acid are decoded by a set of transfer RNAs (tRNAs) called isoacceptors. We report the surprising observation that two isoacceptor tRNAs that decode synonymous codons become modulated in opposing directions during breast cancer progression. Specifically, $tRNA^{Ile}_{UAU}$ became upregulated, whereas $tRNA^{Ile}_{GAU}$ became repressed as breast cancer cells attained enhanced metastatic capacity. Functional studies revealed that $tRNA^{Ile}_{UAU}$ promoted and $tRNA^{Ile}_{GAU}$ suppressed metastatic colonization. The expression of these tRNAs mediated opposing effects on codon-dependent translation of growth promoting genes. Consistent with this, multiple mitotic gene sets in the human genome are significantly enriched in the codon cognate to the growth-promoting $tRNA^{Ile}_{UAU}$ and significantly depleted of the codon cognate to the growth-suppressive $tRNA^{Ile}_{GAU}$. Our findings uncover a specific isoacceptor tRNA pair that act in opposition—divergently regulating genes that contribute to growth and a disease phenotype. The degeneracy of the genetic code can thus be biologically exploited by human cancer cells via tRNA isoacceptor shifts that facilitate the transition towards a growth-promoting state.

Because of the degeneracy of the genetic code, multiple transfer RNAs (tRNAs) bearing distinct anticodons can accept the same amino acid for translational incorporation into the growing polypeptide chain during translation[1,2]. Such tRNA isoacceptors recognize what are called 'synonymous codons'. Transfer RNAs have long been considered static adaptor

molecules that play critical roles in converting the genetic code to an amino acid code. This notion has been revisited in recent years with observations of altered expression of tRNAs in the context of disease[3–5]. Specific tRNAs were observed to become over-expressed or repressed in proliferative cancer cells relative to differentiated cells[5]. Within a set of tRNAs encoding the same amino acid, specific isoacceptors were found to become upregulated while others were found to become repressed in concert with modulation of growth or differentiation related transcripts, revealing potential coordination between tRNAs and their mRNA clients[5]. These findings suggested potential for certain tRNAs to causally impact cancer phenotypes. Indeed, over-expression of the initiator methionine had been found to increase *in vitro* proliferation[6], while tRNA$^{Glu}_{UUC}$, which becomes amplified in breast cancer, was found to promote breast cancer metastatic invasion by enhancing the codon-dependent translation of an invasion gene—comprising a tRNA-regulated pathway[4]. Analogous to these observations, aminoacyl tRNA synthetases (aaRS), responsible for charging tRNAs with cognate amino acids, have been shown to play non-canonical roles[7] and recent work has demonstrated significant cancer progression roles for specific charging enzymes[8,9]. These studies have raised a number of questions, including whether transcriptional deregulation in the absence of tRNA genomic copy number alterations can modulate tRNA levels and cancer progression, whether there exist metastasis suppressor tRNAs in human cancer, and if there exist tRNA pairs that are functionally antagonistic of a given phenotype.

Isoleucyl tRNA isoacceptors are divergently modulated in breast cancer

To identify tRNAs that may become transcriptionally modulated during cancer progression, we performed chromatin immunoprecipitation sequencing (ChIP-seq) in poorly and highly metastatic human breast cancer cells[10] using an antibody targeting the DNA binding subunit of Polymerase III, POLR3A. Enrichment of tRNA loci was confirmed by successful co-immunoprecipitation of Pol III genomic target loci through quantitative real-time PCR (qPCR) (Supplementary Fig. 1a), as well as significant enrichment of ChIP-seq reads for tRNA Box A and Box B gene regulatory sequences (Supplementary Fig. 1b–c). We observed that an isoleucyl-tRNA (TAT) isoacceptor locus that encodes tRNA$^{Ile}_{UAU}$ was significantly more bound by Pol III in highly metastatic MDA-LM2 cells relative to the parental poorly-metastatic MDA-MB-231 cells from which it was derived (Fig. 1a). To confirm these findings and to establish that mature tRNA$^{Ile}_{UAU}$ levels are upregulated in metastatic cells, we performed targeted tRNA profiling by tRNA Capture-seq[4]. Targeted tRNA quantification in the MDA-MB-231 poorly/highly metastatic pair as well as an independent poorly/highly metastatic isogenic human breast cancer line pair (HCC1806-Par and HCC1806-LM2C, validated in Supplementary Fig. 1d) confirmed that mature tRNA$^{Ile}_{UAU}$ is upregulated in highly metastatic breast cancer cells relative to isogenic poorly metastatic cells (Fig. 1b). Northern blot analysis confirmed the observations of tRNA$^{Ile}_{UAU}$ over-expression in highly metastatic breast cancer cells (Supplementary Fig. 1e). Genomic copy number analysis by qPCR did not reveal increased genomic copy number of isoleucyl-tRNA (TAT) loci in highly metastatic cells, consistent with transcriptional enhancement (Supplementary Fig. 1f). In parallel to these observations, we made the surprising observation that one of the other isoacceptors of isoleucine, tRNA$^{Ile}_{GAU}$, became

significantly repressed in the highly metastatic sublines relative to isogenic poorly metastatic parental cells (Fig 1c). The high sequence similarity between $tRNA^{Ile}_{GAU}$ and another isoleucine isoacceptor $tRNA^{Ile}_{AAU}$ precluded specific northern blot quantification for $tRNA^{Ile}_{GAU}$ as an independent tRNA quantification method. We thus employed pre-tRNA quantification as an orthogonal approach for assessing the levels of all three isoleucyl tRNAs. Pre-tRNA qRT-PCR also revealed upregulation of $tRNA^{Ile}_{UAU}$ expression by the multiple genomic loci that encode it and conversely, repression of $tRNA^{Ile}_{GAU}$ loci genes in both pairs of highly metastatic breast cancer cells relative to their isogenic poorly metastatic parental cell populations (Fig 1d–e). We did not observe such global modulations of the third isoleucyl isoacceptor pre-$tRNA^{Ile}_{AAU}$ across the loci surveyed (Supplementary Fig. 1g). In support of these findings, FISH staining of human tissue microarrays of breast cancer patients with locked nucleic acids (LNAs) targeting $tRNA^{Ile}_{UAU}$ and $tRNA^{Ile}_{GAU}$ revealed a significantly increased ratio of $tRNA^{Ile}_{UAU}$/$tRNA^{Ile}_{GAU}$ expression in stage III breast tumours, which exhibit higher rates of metastatic relapse, relative to stage I or stage II tumours, which exhibit lower rates of metastasis (Fig. 1f, Supplementary Fig. 1h). These findings reveal that metastatic progression in breast cancer selects for upregulation of one isoleucyl tRNA isoacceptor and repression of another. This shift in tRNA isoleucyl isoacceptor levels suggests potentially differential roles for these tRNAs in breast cancer progression.

TRNA$^{Ile}_{UAU}$ promotes and tRNA$^{Ile}_{GAU}$ suppresses breast cancer metastasis

To determine if the observed reciprocal tRNA isoleucyl isoacceptor modulations play causal roles in cancer progression, we performed loss-of-function and gain-of-function studies for these tRNA isoacceptors. We first sought to overexpress $tRNA^{Ile}_{UAU}$ in poorly metastatic cells to assess whether its upregulation was sufficient to confer increased metastatic capacity (Supplementary Fig. 2a–b). Stable over-expression of $tRNA^{Ile}_{UAU}$ to pathophysiologically relevant levels (~50% increase) in poorly metastatic MDA-MB-231 or HCC1806 human cell lines significantly increased lung metastatic colonization in tail-vein colonization assays as assessed by bioluminescence imaging and histological analyses (Fig. 2a–b). For loss-of-function studies, we employed CRISPR-Cas9 using two independent guides specific to $tRNA^{Ile}_{UAU}$ genomic loci (Supplementary Fig. 2c). CRISPR-Cas9 mediated depletion of $tRNA^{Ile}_{UAU}$ in highly metastatic MDA-LM2 breast cancer cells to levels similar to poorly metastatic cells was sufficient to significantly impair breast cancer metastatic colonization (Fig. 2c, Supplementary Fig. 2d–e). These findings reveal $tRNA^{Ile}_{UAU}$ to be a promoter of metastatic progression in these human breast cancer cells.

We next determined if $tRNA^{Ile}_{GAU}$, which became repressed in metastatic cells, plays a causal role in breast cancer progression. TRNA$^{Ile}_{GAU}$ was stably overexpressed in highly metastatic MDA-LM2 cells to levels similar to those observed in poorly metastatic MDA-231 parental cells (~1.8-fold over-expression) (Supplementary Fig. 2f). Increasing $tRNA^{Ile}_{GAU}$ expression in highly metastatic MDA-LM2 cells substantially reduced metastatic lung colonization capacity (Fig. 2d). Given the high sequence similarity between $tRNA^{Ile}_{GAU}$ and $tRNA^{Ile}_{AAU}$, we employed two orthogonal approaches for $tRNA^{Ile}_{GAU}$ loss-of-function—CRISPRi and shRNA mediated interference. Firstly, MDA-231 cells were stably transduced with mutant Cas9-KRAB and a specific guide complementary to

common sequences in tRNA$^{Ile}_{GAU}$ genomic loci. Reduced tRNA$^{Ile}_{GAU}$ was confirmed by targeted tRNA capture qPCR (Supplementary Fig. 2g). ShRNA-mediated interference was also employed using a hairpin specific to tRNA$^{Ile}_{GAU}$ (Supplementary Fig. 2h). While tRNA$^{Ile}_{GAU}$ was significantly decreased in expression, there was no significant difference in the abundance of the other isoleucyl tRNAs, tRNA$^{Ile}_{AAU}$ and tRNA$^{Ile}_{UAU}$ (Supplementary Fig. 2i). Depletion of tRNA$^{Ile}_{GAU}$ using both approaches enhanced lung metastatic colonization by poorly metastatic MDA-231 cells (Fig. 2e and 2f). Concurrent modulation of isoleucyl tRNA expression through increased tRNA$^{Ile}_{UAU}$ and decreased tRNA$^{Ile}_{GAU}$ to mimic isoleucyl tRNA expression in highly metastatic cells significantly enhanced metastatic colonization (Fig. 2g, Supplementary Fig. 2j). This was consistently observed, as the impact of dual tRNA$^{Ile}_{UAU}$ /tRNA$^{Ile}_{GAU}$ modulation increased metastasis in two other breast cancer cell lines, HCC1806 and MDA-MB-268 in a xenograft model (Fig. 2h–j, Supplementary Fig. 2k–l). These findings implicate tRNA$^{Ile}_{GAU}$ as a metastasis suppressor tRNA and uncover two surprising findings: the first being a gain-of-function organismal disease phenotype upon depletion of a tRNA (tRNA$^{Ile}_{GAU}$); the second being the observation of a dichotomy between two tRNA isoacceptors in regulating a common phenotype.

To determine whether the effect of isoleucyl tRNA modulation on cancer progression also impacted primary tumour growth, we performed orthotopic mammary fat pad injections with the parental MDA control breast cancer cells as well as the dual tRNA$^{Ile}_{UAU}$ /tRNA$^{Ile}_{GAU}$ modulated cells. We observed no significant difference in primary tumor growth (Fig. 2k), or in the number of circulating tumor cells (Supplementary Fig. 2m–n) upon dual tRNA$^{Ile}_{UAU}$ /tRNA$^{Ile}_{GAU}$ modulation. In contrast, we observed a very substantial (>14-fold by bioluminescence) increase in lung metastatic colonization from the orthotopic mammary gland site (Fig. 2l), confirming the effects we observed for metastasis in tail vein metastatic colonization assays. These data collectively indicate that increased tRNA$^{Ile}_{UAU}$ and repressed tRNA$^{Ile}_{GAU}$ expression drives distal organ breast cancer metastatic colonization, rather than primary tumour growth, intravasation, or survival in the circulation.

TRNA^{Ile} isoacceptors divergently regulate growth and growth gene expression

We next sought to identify the cancer progression cellular phenotype(s) regulated by tRNA$^{Ile}_{UAU}$ and tRNA$^{Ile}_{GAU}$ by searching for gene sets that exhibit enrichments or depletions of codons cognate to these tRNAs. We performed pathway enrichment analyses using the iPAGE framework[11]—assessing significant genome-wide abundances for the codons cognate to tRNA$^{Ile}_{UAU}$ and tRNA$^{Ile}_{GAU}$ in an unbiased manner. All coding transcripts in the human genome were ranked and binned by AUA or AUC relative synonymous codon usage (RSCU). Pathways that were significantly enriched (p<10^{-3}) across discretized bins were identified based on their mutual information content (Fig. 3a–b). Interestingly, transcripts most signficantly enriched in AUA codons (cognate to tRNA$^{Ile}_{UAU}$) were enriched in mitosis related gene sets such as metaphase, anaphase, and chromatid separation, and homologous DNA pairing and strand exchange (Fig. 3a). Conversely, AUC codons (cognate to tRNA$^{Ile}_{GAU}$) were most significantly depleted from

these mitosis related gene sets (Fig. 3b). As an orthogonal and functional approach for identifying the downstream consequences of modulation of these tRNAs, we conducted ribosomal profiling of breast cancer cells in the context of tRNA$^{Ile}_{UAU}$ overexpression and tRNA$^{Ile}_{GAU}$ depletion (by CRISPRi), mirroring the divergent tRNA^{Ile} modulations observed in highly metastatic cells relative to poorly metastatic cells. Ribosomal protected fragments were sequenced, and conformed to the expected size and periodicity reported by other groups[12] (Supplementary Fig. 3a–b). Ribosomal occupancy of transcripts was then quantified as a measure of translational efficiency (Supplementary Fig 3c–d). Genes enriched in GO terms such as cell cycle and mitosis exhibited enhanced translational efficiency (Fig. 3c). At the proteomic level, GO functional analysis of proteins in tRNA$^{Ile}_{UAU}$/tRNA$^{Ile}_{GAU}$ modulated cells by label free mass spectrometric quantification also revealed enrichment of gene sets including cell cycle, mitosis, as well as regulation of stress response relative to control cells (Fig. 3d). Consistent with the growth related gene sets identified using the described approaches, immunofluorescent staining of metastatic nodules for the proliferation marker Ki67 revealed that MDA-MB-231 breast cancer cells concomitantly over-expressing tRNA$^{Ile}_{UAU}$ and depleted of tRNA$^{Ile}_{GAU}$ exhibited greater proliferation than control cells (Fig. 3e). To determine if these *in vivo* observations could be recapitulated *in vitro*, growth assays were performed under normal tissue culture conditions and under conditions of hypoxic and oxidative stress, since such stresses occur in the metastatic microenvironment and can restrict growth[13–18]. Concomitant tRNA$^{Ile}_{UAU}$ upregulation/tRNA$^{Ile}_{GAU}$ depletion enhanced the *in vitro* growth of MDA MB 231 breast cancer cells relative to control cells in the context of hypoxia (Fig. 3f) and oxidative stress (Fig. 3g). Importantly, growth effects were more pronounced under these stress conditions that are known to occur in the tumour microenvironment than under normoxic basal *in vitro* conditions (Supplementary Fig. 3e). These findings reveal that divergent modulation of these isoleucyl tRNA isoacceptors promotes growth in these breast cancer cells *in vivo* and *in vitro*.

A growth gene network regulated by TRNA^{Ile} isoacceptors

We next sought to identify examples of downstream effector genes that could mediate cell growth effects downstream of tRNA$^{Ile}_{UAU}$/tRNA$^{Ile}_{GAU}$ modulation. We hypothesized that there exist growth-promoting genes enriched in AUA codons cognate to tRNA$^{Ile}_{UAU}$. We identified the set of genes that exhibited enhanced translational efficiency as well as enhanced mass-spectrometric protein abundances upon concurrent tRNA$^{Ile}_{UAU}$/tRNA$^{Ile}_{GAU}$ modulation, and exhibited a high relative synonymous codon usage score for tRNA$^{Ile}_{UAU}$. The ten genes that fulfilled these criteria were further restricted to those that exhibited enhanced translational efficiencies and protein abundances in highly metastatic cells, which endogenously modulate these tRNAs relative to the isogenic parental poorly metastatic population (Fig. 3h)[4]. This yielded six genes as candidate downstream growth-promoting effectors (Supplementary Fig. 3f). Functional testing revealed that RNAi-mediated depletion of three of these genes (*SMNDC1*, *LSM6*, and *PYCARD*) reduced proliferation (3i–k, Supplementary Fig. 3g,h). Depletion of each of these genes significantly reduced the enhanced metastatic colonization capacity of the tRNA$^{Ile}_{UAU}$/tRNA$^{Ile}_{GAU}$ dual modulated breast cancer cells, consistent with collective contribution of each of these genes,

which become collectively translationally enhanced upon dual tRNA$^{Ile}_{UAU}$ /tRNA$^{Ile}_{GAU}$ modulation, to the enhanced metastatic phenotype (Fig. 3l). We next focused on one gene, *SMNDC1*, for mutagenesis studies (Supplementary Fig. 3i). To determine if isoleucyl tRNA modulations could directly enhance translation of a growth-promoting gene in a codon-dependent manner, we employed a reporter-based approach in which AUA codons in *SMNDC1* were mutated to synonymous AUC codons. While the wildtype SMNDC1 protein became upregulated upon dual tRNA modulation, synonymous codon mutant SMNDC1 protein levels remained unchanged (Fig. 3n–o)—consistent with codon-dependent tRNA$^{Ile}_{UAU}$-driven enhancement of translation of this growth-promoting gene. We similarly confirmed the enhanced expression of wild-type PYCARD in tRNA$^{Ile}_{UAU}$ /tRNA$^{Ile}_{GAU}$ cells, which was in turn abrogated in AUA-to-AUC PYCARD mutants (Supplementary Fig. 3j). These findings reveal that divergent isoleucyl tRNA modulation enhances translation of a set of growth-promoting genes with high tRNA$^{Ile}_{UAU}$ relative synonymous codon usage scores.

Divergent tRNA isoacceptor modulation impacts ribosomal function

The opposing directionality of the metastasis phenotype observed upon modulating these isoacceptor tRNAs suggests that they may elicit distinct downstream codon-dependent translational effects at a global level. To test this, we performed polysome profiling studies (Supplementary Fig. 4a). This revealed that relative to control cells, concurrent tRNA$^{Ile}_{UAU}$ over-expression and tRNA$^{Ile}_{GAU}$ depletion elicited a significant increase in polysome occupancy of transcripts enriched in the AUA codon, which is cognate to the over-expressed tRNA$^{Ile}_{UAU}$ (z-score 23.6; robustness 10/10; Fig. 4a) and a reduction in actively translating transcripts enriched in the AUC codon, which is cognate to the depleted tRNA$^{Ile}_{GAU}$ (z-score 44.8; robustness 10/10; Fig. 4b). This translational modulation was further tested in gene candidates SMNDC1 and EPHX1. In MDA cells with concurrent tRNA$^{Ile}_{UAU}$ over-expression and tRNA$^{Ile}_{GAU}$ depletion relative to control, SMNDC1 was up-regulated ~2-fold in the polysome associated fraction, while EPHX1, which is predicted to be repressed translationally by these tRNAs, was similarly down-regulated (Supplementary Fig. 4b). Consistent with this, analysis of the aforementioned ribosomal profiling data revealed that upon dual tRNA$^{Ile}_{UAU}$/tRNA$^{Ile}_{GAU}$ modulation, there was also a significant enrichment of ribosomal occupancy of AUA-containing transcripts and reduced occupancy of AUC-containing transcripts (Supplementary Fig. 4c,d). Our findings as a whole suggest a model whereby tRNA$^{Ile}_{UAU}$/tRNA$^{Ile}_{GAU}$ modulation enhances the efficiency of AUA codon decoding by the ribosome. This would suggest that we should observe reduced ribosomal dwell time over AUA codons upon dual tRNA modulation. Moreover, we would expect to see increased binding of tRNA$^{Ile}_{UAU}$ relative to tRNA$^{Ile}_{GAU}$ to the ribosome upon tRNA$^{Ile}_{UAU}$/tRNA$^{Ile}_{GAU}$ modulation. In order to capture the dwell time of ribosome at every codon, we measured the extent to which its occupancy in the ribosome profiling data deviates from its predicted level based on loess regression[19]. We observed that tRNA$^{Ile}_{UAU}$/tRNA$^{Ile}_{GAU}$ modulation significantly reduced ribosome dwell time over AUA codons, consistent with productive translation, while over-expression of tRNA$^{Ile}_{UAU}$ or depletion of tRNA$^{Ile}_{GAU}$ individually were insufficient to elicit significant shifts in dwell time (Fig. 4c). To determine if tRNA modulations impact ribosome-associated

$tRNA^{Ile}_{UAU}$ and $tRNA^{Ile}_{GAU}$ abundances, we quantified the abundance of these tRNAs from polysomal ribosomes as well as total cellular input. We observed that $tRNA^{Ile}_{GAU}$ depletion reduced the ribosomal association of this tRNA, while $tRNA^{Ile}_{UAU}$ over-expression enhanced its ribosome association (Fig. 4f). Importantly, dual $tRNA^{Ile}_{UAU}/tRNA^{ile}_{GAU}$ modulation caused the greatest increase in relative $tRNA^{Ile}_{UAU}$ to $tRNA^{Ile}_{GAU}$ ribosomal association (Fig. 4g). The substantially increased ribosomal association of $tRNA^{Ile}_{UAU}$ upon dual $tRNA^{Ile}_{UAU}/tRNA^{Ile}_{GAU}$ modulation relative to $tRNA^{Ile}_{GAU}$ depletion supports the translational consequences observed upon polysome profiling (Fig. 4d, e). These concordant observations of global shifts in isoleucine codon enrichments and depletions in polysome profiling and ribosomal profiling studies as well as dwell time and biochemical analyses support direct codon-dependent effects on translation upon divergent modulation of these tRNAs. Our findings as a whole support a model whereby isoleucyl isoacceptor tRNA abundance shifts impact codon-dependent translation of growth regulating genes at the ribosome, thereby promoting cancer progression (Fig. 4h).

Discussion

Our observations reveal opposing roles for two isoleucyl tRNAs that are transcriptionally deregulated during breast cancer progression in regulation of breast cancer metastatic colonization and cancer cell growth. Our findings as a whole support a model whereby shifts in $tRNA^{Ile}$ isoacceptor abundance impact codon-dependent translation of growth regulating genes at the ribosome, thereby promoting cancer progression (Fig. 4h). The molecular and functional studies implicating growth as a phenotype divergently impacted by modulation of these tRNAs is supported by genome sequence analyses that reveal significant enrichment or depletion of the codons cognate to these antagonistic tRNAs in mitotic gene sets. Future studies are warranted to better elucidate the molecular basis of such interferences and to search for additional examples of such antagonistic isoacceptor tRNA pairs in health and disease.

Methods

Cell Culture

MDA-MB-231 and its highly metastatic derivative[10] LM2 cells were cultured with DMEM media supplemented with 10% FBS, sodium pyruvate, and L-glutamine. HCC1806 Parental and derivate cell lines were cultured in 1x RPMI supplemented with 10% FBS, sodium pyruvate, 1mM HEPES as specified by ATCC. All cell lines were regularly tested for mycoplasma infection and were negative. Each cell line was verified using STR testing, performed by the Integrated Genomics Operation at MSKCC. Cells were retrovirally transduced with a luciferase reporter for bioluminescence detection as previously described[4,15,20]. Oxidative stress analyses were conducted by addition of 200 uM hydrogen peroxide to cells.

In Vivo Selection

Several female Nod SCID Gamma (NSG) (Jackson # 005557) mice were injected at 6 weeks of age intravenously via tail vein with 150,000 parental HCC1806 cells and monitored by

bioluminescence IVIS imaging (IVIS Lumina II) until photon flux of lungs reached $10^{\wedge}7$ or $10^{\wedge}8$ (4–7 weeks). Subsequently, animals were euthanized according to IACUC protocol and guidelines, and the lungs were extracted under sterile conditions. The lungs were then placed on a sterile 6cm tissue culture dish and minced with razor blades. Lung tissue extracts were resuspended in 20 mL RPMI Media supplemented with FBS, sodium pyruvate and HEPES with 15 mg/mL Collagenase IV (Worthington). Cells were incubated at 37°C for 30 minutes on a shaker to allow for digestion. Tissue extracts were then spun down at 1000 RPM for 5 minutes at 4°C and resuspended in RPMI media without Collagenase IV. Cells were filtered with a 100 um filter (Corning) and spun down again. Cells were then treated with 5 mL ACK Lysis Buffer and left at room temperature for 5 minutes. Cells were spun again and resuspended in 1 mL Optiprep solution 1 (2:1, Optiprep:Media). A gradient was constructed with an additional 4 mL Solution 1, overlain by 3 mL Optiprep Solution 2 (2.2:1, Solution1: Media). 1 mL Media was overlain and the gradient was spun down for 20 minutes at 1000 RPM 4°C. Viable cells were collected from the top of the gradient and washed twice with RPMI media. Cells were then plated in 75 cm filtered flasks with PenStrep and Fungizone added to the RPMI Media. The cells were cultured for approximately a week to reduce stromal cell survival and then tested for mycoplasma. To generate an in vivo selected line twice, these lung metastatic 1 (LM1) generation cells were then re-injected at 150,000 tail vein and the process was repeated.

Chromatin Immunoprecipitation

MDA-MB-231 and LM2 cells in biological replicates were plated in 15 cm plates (~12 million cells). For cross-linking, 1% formaldehyde was added to cells at 37°C for 10 minutes, and quenched with glycine at a final concentration of 0.14 M for 30 minutes at room temperature. The plates were put on ice, the media was removed and cells were washed with ice cold PBS twice. 500 uL PBS with 1x HALT protease inhibitors (Thermo) were added and cells were scraped and put in an Eppendorf on ice. Cells were pelleted at 4000 RPM in a refrigerated centrifuge for 4 minutes. The cell pellets were then resuspended in 400 uL Lysis buffer (1% SDS, 50 mM Tris Hcl pH 8.0 20 mM EDTA, protease inhibitors (Roche) and incubated on ice for 10 minutes. Lysates were then sonicated to produce DNA fragments between 200 – 1000 bp with settings Amplitude 70, 10 sec on 30 sec rest for three repetitions on Sonicator S-4000 (Branson) with Microtip and Ultrasonic Liquid Processor (Misonix). Lysates were kept on ice during sonication to prevent protein degradation. Lysates were then clarified by centrifugation at max speed at 4 °C for 10 minutes. Equivalent amounts of lysate were then added to separate eppendorfs, saving some lysate for input samples. Either 5 ug rabbit IgG or 5ug POLR3A (Cell Signaling #12825S) were then added, with a final volume of 1 ml with protease inhibitors of dilution buffer (16.7 mM Tris HCl pH 8.0, 0.01% SDS, 1.1% Triton X-100, 1.2 mM EDTA, 167 mM NaCl). Lysate and antibody mixtures were incubated overnight at 4 °C with rotation. 50 uL Protein G Dynabeads were added to each sample after washing and incubated at 4 °C for 2 hours with rotation. Tubes were then placed on a magnet for 2 minutes, discarding the supernatant. The following washes were performed, twice each for 5 minutes at 4 °C in the following order: low salt (140 mM NaCl, 50 mM HEPES, 0.1% SDS, 1% Triton X-100, 0.1% deoxycholate, 1 mM EDTA) high salt (500 mM NaCl, 50 mM HEPES, 0.1% SDS, 1% Triton X-100, 0.1% deoxycholate, 1 mM EDTA), LiCl (250 mM LiCl, 20 mM

Tris HCl pH 8.0, 0.5% NP-40, 0.5% deoxycholate, 1 mM EDTA) and TE Buffer (10 mM Tris HCl pH 8.0, 1 mM EDTA). 100 uL Elution buffer (50 mM Tris HCl pH 8.0, 1 mM EDTA) was then added to the beads and incubated overnight at 65 °C on a shaker to enable elution. The eluted sample was transferred to a new tube and repeated for a final volume of 200 uL per sample. 1 uL of 10 mg/mL RNase A was added to each sample (including input samples) and incubated at 37 °C for 30 minutes. 2 uL of Proteinase K was added (10 mg/mL) and incubated for 2 hours at 56 °C. DNA was then purified using the DNA Clean and Concentrator Kit (Zymo Research). Enrichment of Polymerase III bound loci was confirmed with genomic tRNA qPCR primers and quantified as Percent Input over IgG. The Input and IP DNA samples were then PCR amplified with Illumina barcodes to construct a multiplexed library. The library was quantified using TapeStation and sequenced on the 50 SR HiSeq at the Rockefeller Genomics Resource Center.

tRNA Capture qPCR

tRNA quantification by RT-qPCR was performed as described previously[1]. RNA purified with Norgen Total Purification Kit was quantified using a Nanodrop. Normalized RNA across samples was added to a hybridization mixture (final concentration 10 mM Tris HCl pH 7.4, 50 mM NaCl, 1 mM EGTA pH 8.0) with 2 uM Hybridization probes. Hybridization probes specific for the following tRNA were used: Ile TAT Left 5' /5Phos/ AAGTACCGCGCGCTACCGATTGCGCCACTGGAGCGATCGTCGGACTGTAGAA, Ile TAT Right 5 CGTGTGCTCTTCCGATCTTGCTCCAGGTGAGGCTCGAACTCACACCTCGGCATTAT ', Ile GAT Left 5' /5Phos/ CAGCACCACGCTCTACCAACTGAGCTAACCGGCCGATCGTCGGACTGTAGAA, Ile GAT R 5' CGTGTGCTCTTCCGATCTTGGCCGGTGCGGGAGTCGAGCCCGCGCCTTGGTGTTA T 3'. Each 'left' probe contained a 5' phosphate to enable subsequent ligation. RNA and probe mixture was hybridized using a thermocycler and brought to RT. 1x SplintR ligase buffer, SplintR Ligase (NEB) and RNase Inhibitor (Promega) were added and incubated at room temperature for 2 hours. An additional ligation step with T4 Ligase was performed overnight at 16 °C. The RNA was then degraded with RNase A (Thermo Fisher) & H (NEB) for 30 minutes at 37 °C. The ligated probe reaction was then diluted 1:50 and quantified using primers (Forward 5' CGTGTGCTCTTCCGATCT 3' & Reverse 5' GATCGTCGGACTGTAGAA 3') specific to the probe backbone by RT-qPCR. 5S and 18S probes were used as loading controls: 5S Left 5' 5PHOS/ CTGCTTAGCTTCCGAGATCAGACGAGATCGGGCGCGATCGTCGGACTGTAGAA 3' 5S Right 5' CGTGTGCTCTTCCGATCTCCAGGCGGTCTCCCATCCAAGTACTAACCAGGCCCGA CC 3' or 18S Left 5' 5PHOS/ CCTAGTAGCGACGGGCGGTGTGTACAAAGGGCGCCGATCGTCGGACTGTAG 3' 18S Right 5' CGTGTGCTCTTCCGATCTCCGATCCGAGGGCCTCACTAAACCATCCAATC 3'.

Northern Blot

RNA was purified using Norgen total RNA Purification kits according to manufacturer's instructions. 5 ug purified RNA was run on 10% TBE-Urea gels at 200V for 1 hour, and transferred to a Hybond-N+ membrane (GE) at 150A for 1 hour. RNA was then crosslinked to the membrane at 240 mJ/cm^2, and blocked with Oligo Hybridization Buffer (Ambion) for 1 hour at 42 °C. Northern probes were labeled with ^{32}P ATP with T4 PNK (NEB), purified with a G25 column (GE Healthcare), and hybridized in Oligo Hybridization Buffer overnight at 42 °C. Membranes were washed with 2X SSC 0.1% SDS Buffer, then with 1X SSC 0.1% SDS Buffer. Films were developed at varying times subject to radioactivity of membrane. Probe oligo sequences for Ile TAT Intron: 5' ACUGCUGUAUAAGUACCGCGCGC 3' and Ile TAT 5' cucggcauuauaaguaccgcgcgc 3' and U6 5' CACGAATTTGCGTGTCATCCTT 3'. Membranes were stripped with 0.1% SDS in boiling water and allowed to cool to room temperature. Quantification was performed with ImageJ and normalized to U6 levels.

RT qPCR

RNA was purified using the Norgen total RNA Purification kits according to manufacturer's instructions. 1ug purified RNA was used for cDNA production with Superscript III reverse transcriptase (Thermo Fisher Scientific) using random hexamer as a template. The cDNA was diluted 1:5 and quantified with Sybr Green Master Mix (Thermo). The ddCT levels were quantified through normalization to 18S with biological replicates. One primer set was used for tRNA$^{Ile}_{GAT}$ genetic loci chr.X-6 and chr.X-7 as their sequences are indistinguishable. Primer sequences are available in the Supplemental Material Section.

tRNA Fluorescence In Situ Hybridization

Breast tissue microarrays were obtained from Biomax (BC08118 & BR1005b). Slides underwent deparaffination via 5 minute incubations in xylene 2x, 100% Ethanol, 2x, 70% Ethanol, 50% Ethanol, and subsequently molecular grade water. Antigen retrieval was performed with 1x Citrate Buffer pH 6.0 in a microwave for 20 minutes. Slides were cooled to room temperature, then tissue regions were isolated with a PAP pen. Slides were incubated in 0.13 M 1-methylimidizaole 300 mM NaCl pH 8.0 solution twice for 10 minutes each. Next, slides were incubated with 0.16 M N-(3-Dimethylaminopropyl)-N-ethylcarbodiimide hydrochloride (EDC) (Sigma Aldrich) in the 1-methylimidazole solution for 1 hour at RT to preserve small RNAs[21]. Slides were then washed with 0.2% Glycine in Tris buffered saline (TBS) pH 7.4, then in TBS twice. Pre-hybridization of slides occurred with 1X ISH (Exiqon) buffer at 53 °C for 1 hour. 40 nM tRNA double DIG labeled LNA Probe targeting tRNA$^{Ile}_{UAU}$ (Sequence 5' CA+GGTGAGGCTCGAACTCACAC+C+TCGGCAT+T+A 3' with +N indicating LNA at that nucleotide) and tRNA$^{Ile}_{GAU}$ (Sequence 5' AGTCGA+GCCCGCGAC+CTTGG+TGTTA+T+C 3') (Qiagen) in 1X ISH buffer was denatured at 95°C for 5 minutes followed by cooling on ice for 1 minute. The LNA probe was added to the slide (and covered with a glass coverslip to prevent evaporation) and hybridized overnight at 52 °C. Slides were then washed with 4X SSC, 2X SSC, 1X SSC, and 0.5X SSC in 50% formamide for 20 minutes each, then washed with 100 mM Tris-HCl

pH 7.4 150 mM NaCl (TN buffer) for 5 minutes. Slides were blocked with 1X Blocking Reagent (Roche) in TN buffer for 1 hour at RT. Anti-DIG POD in TN blocking buffer was added 1:100 and incubated for 2 hrs. Slides were washed 3x for 5 minutes in TN buffer with 0.05% Tween-20 (TNT). FITC-tyramide solution 1:100 in 1x amplification reagent (TSA) was incubated on slides for 10 minutes at RT. Slides were subsequently washed 3x for 5min with TNT buffer. Samples were washed with PBS and stained with DAPI for 5 minutes, then mounted with Prolong Gold anti-fade solution (Thermo Fisher). Fluorescent intensity was measured on an Inverted TCS SP8 laser scanning confocal microscope (Leica) at the Bioimaging Resource Center at Rockefeller University and quantified by mean fluorescence intensity relative to DAPI. Quantification was performed blind.

Viral Production & Stable Cell Line Generation

Stable generation of cell lines was performed as previously described[1,6,7]. Lentivirus was generated using the ViraSafe lentiviral packaging system (Cell Biolabs) with Lipofectamine 2000 (Invitrogen) in HEK293T cells. Transductions were performed with 8 ug/mL polybrene. Plasmids to overexpress $tRNA^{Ile}$ or with shRNAs targeting $tRNA^{Ile}_{GAU}$ were cloned into the plko.1 puromycin (Addgene # 8453) or blasticidin (Addgene #26655) backbone with AgeI/EcoRI restriction sites[22,23]. CRISPRi stable cells lines were generated with lentiviral transduction of dCas9-KRAB (Addgene # 110820) and pSLQ plasmid (Addgene # 51024) cloned with a $tRNA^{Ile}_{GAU}$ targeting guide (5' TGAGCTAACCGGCCGCCCGA 3'), and then flow sorted for positive BFP+ and mCherry+ cells[24,25]. CRISPR generated cells were transduced with lentiCRISPRv2 (Addgene # 98290) cloned with specific guides targeting $tRNA^{Ile}_{UAU}$ loci (Guide 1: 5' GCGCTAACCGATTGCGCCAC 3', Guide 2: 5' TGGCGCAATCGGTTAGCGCG 3') or the eGFP targeting sequence as control (5' GGGGCGAGGAGCTGTTCACCG 3'). Cells were then either selected with 2 ug/mL puromycin or 7.5 ug/mL Blasticidin (Thermo Fisher Scientific).

Animal Studies

For metastasis assays, tail veins injections were performed in 5–6 week age matched female NOD SCID Gamma mice (The Jackson Laboratory #005557). Cells were counted via hemacytometer and resuspended in 1x PBS, and 100uL was injected with a 27G ½ needle (BD) into the lateral tail vein. Non-invasive bioluminescence imaging was performed immediately after injections using an IVIS Lumina II (Caliper Life Science) for Day 0 baseline, followed by weekly imaging. Bioluminesence imaging was obtained through retro-orbital injection of 50uL D-luciferin (Perkin Elmer) followed by 1 minute exposure in IVIS Lumina II. Unless otherwise stated, each experimental group consisted of n=5 mice. For bioluminescence imaging, cell lines were transduced with triple reporter and FACS sorted for GFP positive cells 48hours post transduction[4,10]. All animal work was conducted in accordance with protocols approved by the Institutional Animal Care and Use Committee at The Rockefeller University.

Histology

Lungs were prepared by perfusion fixation with 4% paraformaldehyde through the circulation via the right ventricle post euthanasia. Lungs were then fixed in 4%

paraformaldehyde overnight at 4°C. The samples were then embedded in paraffin and sectioned in 5 μm slices that were used for immunostaining. 5 μm sections at different depths were stained with hematoxylin and eosin (H&E).

Ribosomal Profiling

Ribosomal profiling was performed based on the McGlincy & Ingolia protocol[4]. Briefly, cells were plated in 15 cm dishes at 50% confluency the day before collection. The media was aspirated, and the cells were washed with 5 mL ice cold PBS, and aspirated. The plate was then submerged in liquid nitrogen to freeze the cells. 400 uL ice cold lysis buffer was added to the plate, and scraped immediately. Each lysate was kept on ice until all plates were collected. Several plates were combined with lysis buffer totaling 1 mL per biological replicate. Lysates were then triturated ten times with a 26 gauge needle. Lysates were clarified at top speed for 10 mins in a cold bench top centrifuge and the supernatant was recovered and snap frozen in liquid nitrogen, then stored at −80 °C. Lysates were quantified with Quant-iT Ribogreen assay (Life Technologies) and 60 ug total RNA per sample was incubated with 3 uL RNase I (Epicentre #N6901K) for 45 minutes at RT with light shaking. 10 uL SUPERase*In RNase Inhibitor (Invitrogen) was added to stop digestion, and the RNA was transferred to a 13 mm × 51 mm polycarbonate ultracentrifuge tube. 900 uL Sucrose cushion (1 M Sucrose with 20 U/mL SUPERase*In in polysome buffer[4]) was underlaid and spun at 100,000 RPM at 4°C for 1 hour. With ribosomes pelleted, the supernatant was pipetted out of the tube. 300 uL Trizol was added to the pellet and resuspended. RNA was subsequently purified with the Direct-zol kit (Zymo). RNA was then precipitated overnight and resuspended after ethanol washes in 5 uL 10 mM Tris HCl pH 8.0. Ribosome footprints were isolated after running a 15% TBE-Urea gel and the RNA was excised within the range of 17nt – 34nt and then precipitated overnight. RNA fragments were then dephosphorylated with T4 PNK and ligated to a DNA linker with T4 Rnl2(tr) K227Q (NEB #M0351S) for 3 hours with distinct linker barcodes. Unligated linkers were depleted with yeast 5'-deadenylase (NEB #M0331S) and RecJ exonuclease (Epicentre #RJ411250) at 30°C for 45 minutes. Ligations were then purified with the Oligo Clean & Concentrater kit (Zymo) and samples were pooled. Ribo Zero Gold was then used to deplete ribosomal RNAs (2 reactions were used, and the 50°C step was omitted, Illumina). RNA was then purified using Oligo Clean & Concentration kit. The pooled ligations were then reverse transcribed using Superscript III at 55°C for 30 minutes, with RNA templates hydrolyzed by 2.2 uL 1 M NaOH. Samples were purified with the Oligo Clean & Concentrator kit and run on a polyacrylamide gel and the RT product was excised above 76nt. Gel slices were incubated with DNA gel extraction buffer overnight after the gel was broken up with gel breaker tubes (IST Engineering) and precipitated overnight. The RT product was resuspended in 10mM Tris HCl pH 8.0 and circularized with CircLigase II at 60°C for 1 hour. qPCR quantification of circulization products were performed to quantify number of cycles sufficient for library preparation, with the concentration estimated at 713 pM. 8 cycles were used to amplify the library with Pfusion with the primers indicated, NI-799 and NI-798[4]. Products were purified and size selected at >136bp, primarily at 160bp. The library was then precipitated, quality checked with Tapestation and sequenced on the NextSeq High Output 75 Single Read at the Rockefeller University Genomics Resource Center. Concurrently 1 ug total RNA was prepped for RNA sequencing according to the manufacturer's instructions (Illumina).

Analysis was performed as described previously[1]. For analysis, reads were first subjected to linker removal and quality trimming (cutadapt v1.14). The reads were then aligned against a reference database of rRNAs (iGenomes: AbundantSequenes) and tRNAs (GtRNAdb, hg38) so as to remove contaminants (using bowtie 2.3.4.1). STAR v2.5.2a was then used to align the remaining reads to the human transcriptome (build hg38). Xtail was used to count ribosome protected fragments, estimate translation efficiency, and perform statistical comparisons[26].

Polysome Profiling

Polysome profiling was adapted from Gandin et. al.'s protocol and with direction and assistance from Dr. Alison Ashbrook in Dr. Charlie Rice's laboratory[27]. The day before cell collection, 7.5 million MDA-231 were plated in 15 cm plates (2 plates per experimental biological replicate) in normal DMEM media supplemented with 10% FBS. Cells were plated to achieve approximately 80% confluency at collection time to optimize polysome content. Each plate was treated for 5 minutes at 37 °C with DMEM with 100 ug/mL cycloheximide. The plate was then transferred to ice and the cycloheximide media was aspirated. Cells were washed twice with ice cold 1x PBS with 100ug/mL cycloheximide. All PBS was then aspirated carefully and the 15 cm plate was flash frozen in liquid nitrogen. 425 uL Lysis Buffer (5 mM Tris HCl pH 7.5, 2.5 mM MgCl2, 1.5 mM KCl, 100 ug/mL cycloheximide, 2 mM DTT, 0.5% Triton X-100, 0.5% sodium deoxycholate, and 100 units of SUPERase*In RNase Inhibitor (Invitrogen) 1x Protease Inhibitors EDTA-free) was then added to the plate and cells were scraped and transferred to an eppendorf tube on ice. Lysates were then spun at high speed at 4°C for 7 minutes to pellet nuclei. Supernatant was transferred to a new tube and the RNA concentration was measured using the Quant-iT Ribogreen assay (Life Technologies). 64ug RNA lysate was used for polysome fractionation. 10–50% Sucrose gradients were prepared the day before ultracentrifugation. Ultracentrifuge polyallomer tubes (Beckman Coulter, Cat #331372) were marked halfway and ~5.5 mL 10% sucrose polysome gradient buffer (20 mM Tris HCl pH 7.5, 140 mM KCl, 5 mM MgCl2, 10% Sucrose, 100 ug/mL cycloheximide, 0.5 mM DTT, 20 U/mL SUPERase*In) was added with a 10 mL sterile syringe to 1/8 inch above the line. 50% sucrose polysome gradient buffer (20 mM Tris HCl pH 7.5, 140 mM KCl, 5 mM MgCl2, 50% Sucrose, 100 ug/mL cycloheximide, 0.5 mM DTT, 20 U/mL SUPERase*In) was then underlain until the 10% sucrose layer was pushed above the marked line. The syringe was wiped with a Kimwipe prior to addition of 50% sucrose buffer to maintain separation between buffers. Black caps were added carefully to prevent the accumulation of bubbles in each ultracentrifuge tube. The Biocomp gradient master was then used at the following conditions: Long Cap 10% - 50% WV Step 1, 1:50 minutes, 80° angle, 21 speed. Gradients were then sealed with parafilm and incubated at 4°C overnight. Gradients were then balanced to within 10mg of each other. Normalized cell lysates were added (500 uL volume) and spun in a SW41 ultracentrifuge rotor at 38,000 RPM for 2 hours at 4°C. 60% sucrose was then used to fractionate spun lysates into 1 mL fractions and polysome peaks were measured with a Combi Flash UV-vis detector (Brandel) and TracerDAQ software. Polysome fractions were then pooled into appropriate groups: highly translated (Higher than 3 ribosomes, past the 1st peak), and lowly translated (1–2 ribosomes and 80s) based on A280 UV peaks. The pooled fractions were then incubated with 3:1 Trizol LS Reagent, vortexed thoroughly,

and incubated at RT for 5 minutes. RNA was then extracted following the instructions of the Direct-zol Miniprep Ki (Zymo Research), and eluted in 50 uL. RNA was quantified and normalized for input into either tRNACapture-seq qPCR with 5S, tRNA$^{Ile}_{GAU}$, or tRNA$^{Ile}_{UAU}$ probes (250 ng) or as Input into the QuantSeq 3' mRNA-Seq Library Prep Kit (Lexogen) kit. 500 ng RNA was used as input and samples were processed according to QuantSeq (Lexogen) instructions. A pooled library was compiled using manufacturer's primers and 10 nM Pool was quality checked with Tapestation and sequenced on the NextSeq High Output 75 Single Read at the Rockefeller University Genomics Resource Center.

For analysis, reads were mapped to the human transcriptome using STAR (v2.5.2a) with genome build hg38 and the number of reads for each gene was tabulated using featureCounts (v1.6.1). The Bioconductor package DESeq2 was then used to compare the fractions in control and tRNA$^{Ile}_{GAU}$/tRNA$^{Ile}_{UAU}$ modulated samples.

Polysome profiling of Specific Targets

Polysome profiling was done with assistance from Dr. Duygu Kuzuoglu-Öztürk in Dr. Davide Ruggero's laboratory. The day before cell collection, 7 million cells were plated per 15 cm plate (2 plates per experimental biological replicate) to achieve approximately 80% confluency at collection time to optimize polysome content. Two hours prior to harvesting, cells were given fresh media. Each plate was then treated for 3 minutes at 37 °C with DMEM with 100 ug/mL cycloheximide. The plate was then transferred to ice and the cycloheximide media was aspirated. Cells were washed twice with ice cold 1x PBS with 100ug/mL cycloheximide, scraped, pelleted, and flash frozen in liquid nitrogen. Frozen cell pellets were thawed and resuspended in 250 uL Lysis Buffer (10 mM Tris HCl pH 8, 140mM NaCl, 1.5 mM MgCl2, 0.25% IGEPAL CA-630, 0.15 mg/mL cycloheximide, 20 mM DTT, 0.1% Triton X-100, and 100 units of RNasin) and incubated on ice for 30 min. Lysates were then spun at 10,000g at 4 °C for 10 minutes to pellet nuclei. Supernatant was transferred to a new tube and the protein concentration was measured using the Pierce BCA Protein Assay Kit (Thermo Scientific). To make the sucrose gradients, ultracentrifuge polyclear tubes (Seton Scientific, Cat #7030) were marked halfway and ~5.5 mL 10% sucrose polysome gradient buffer (25 mM Tris HCl pH 7.4, 25 mM NaCl, 5 mM MgCl2, 10% Sucrose, 2 mM DTT) was added with a 10 mL sterile syringe to the line. 50% sucrose polysome gradient buffer (25 mM Tris HCl pH 7.4, 25 mM NaCl, 5 mM MgCl2, 50% Sucrose, 2 mM DTT) was then underlain until the 10% sucrose layer was pushed above the marked line. The 10–50% Sucrose gradients were prepared with the Biocomp Instruments gradient maker. Cleared lysates (2.6mg of protein) were layered on top of the gradients. The tubes were balanced and spun in a Beckman L8–80M ultracentrifuge with Swinging-Bucket SW 41 rotor at 38,000 RPM for 2.5 hours at 4°C. Samples were separated with the BioComp Instruments fractionator. RNA was extracted from each fraction, except the first 3, following the instructions of the Quick-RNA 96 kit (Zymo Research). RNA was quantified and normalized for input into cDNA synthesis and qPCR analysis.

Proteomics

Cells were lysed in 20 mM Tris HCl pH 8.0, 1% NP-40, 2 mM EDTA with 1x protease inhibitors (Roche). 50 ug lysate was used for label free quantification at the Rockefeller University Proteomics Core Facility. Maxquant software was utilized to compare three replicates per experimental group. Label free quantitation (LFQ) was used to compare the same peptide/protein between experimental groups (n=3 samples per group), which relies on normalization and strict filter criteria determined by the Proteomics Core. Student's t-test difference and student's t-test was then used to analyze the data.

Immunofluorescence

Paraffin embedded histology slides from metastatic nodules were used. Slides underwent deparaffination via 5 minute incubations in xylene 2x, 100% Ethanol, 2x, 70% Ethanol, 50% Ethanol, and subsequently 1x PBS. Antigen retrieval was performed with 1x Citrate Buffer pH 6.0 in a microwave for 20 minutes. Slides were cooled to room temperature, then tissue regions were isolated with a PAP pen. Slides were then blocked with 10% Goat Serum (Sigma Aldrich) for 30 minutes at room temperature. Primary antibodies were incubated overnight at 4°C in a moist chamber (Vimentin V9 mouse (Abcam ab8069) 1:50), or for 2 hours at room temperature (Ki67 (Abcam ab927420) 1:200). Slides were washed with 0.5% Tween 20 PBS then incubated with secondary antibody for 1 hour at RT (1:200). Slides were then stained with DAPI for 5 minutes, and sealed with Prolong Gold anti-fade solution (Thermo Fisher). Fluorescent intensity was measured on an Inverted TCS SP8 laser scanning confocal microscope (Leica) at the Bioimaging Resource Center at Rockefeller University and quantified by number of positive cells per field of view. Quantification was performed blind.

In Vitro Growth Assays

Cells at similar confluencies were resuspended in new DMEM media and counted with a hemacytometer. Cells were then seeded in equal numbers (100K for stress conditions, 50K for normal in vitro conditions) in 6 well plates in triplicate. Cells were then counted at the endpoint day with a hemacytometer. Each experiment was conducted three times. Cells treated with 200 uM H202 were counted on Day 3. Cells exposed to 0.5% hypoxia in an InvivO^2 chamber (Baker Ruskinn) were quantified on Day 3. Growth assays in normal *in vitro* conditions were quantified on Day 5.

Western Blot

Cells seeded a day previously were washed with 1x PBS and then lysed with either RIPA buffer or 20 mM Tris HCl pH 8.0, 1% NP-40, 2 mM EDTA with 1x protease inhibitors (Roche). Protein concentrations were quantified with a BCA Kit (Thermo Fisher) and normalized. Protein lysates were run at 200V for an hour through either a 4–12% Bis-Tris or 3–8% Tris Acetate gel (Invitrogen), and then transferred at 300 mA for one hour in 15% methanol 1x Transfer Buffer on a methanol activated PVDF membrane. Membranes were then stained with Ponceau and blocked for one hour in Odyssey® Blocking Buffer. Primary antibody incubations occurred overnight at 4°C on a rocker at the following concentrations: alpha tubulin 1:1000, (Proteintech) SMNDC1 1:500 (Proteintech). Membranes were then

washed with 0.05% Tween 20 PBS three time and incubated with mouse or rabbit fluorescent IRDye® conjugated secondary antibodies 1:20,000 (LI-COR Biosciences) for one hour. Membranes were subsequently washed three times and imaged and quantified using the Odyssey® Sa Infrared Imaging System at the Rockefeller University Center for High Throughput Screening. Quantification was done using the Image Studio Lite™ software.

Codon Reporters

Wildtype or codon mutant SMNDC1 (all AUA codons changed to AUC codons) coding sequence gene blocks were designed with NheI & XhoI restriction sites and a N-terminal flag tag and ordered from IDT. SMDNC1 gene blocks were cloned into the psiCheck 2 vector. The firefly luciferase was removed and replaced with a renilla luciferase with only AUU encoding isoleucines via restriction cutting with PspOMI & XbaI. This adapted SMNDC1 reporter was transfected with 2.5 ug plasmid and 10 uL Lipofectamine 2000 (Thermo Fisher) in triplicate in MDA-MB-231 cells with modulated tRNA^{Ile} levels. Cells were lysed after 24 hours and protein was extracted with RIPA buffer with 1x protease inhibitors EDTA-free (Roche). Protein expression was measured through LICOR Western blotting as described above.

To quantify the expression levels of wildtype and codon-mutant PYCARD (all AUA codons changed to AUC codons), we generated eGFP–split mCherry fluorescence reporters of wildtype and codon-mutant PYCARD constructs (eGFP –CMV promoter – hPGK promoter – PYCARD (widtype or codon mutant) – GSGSG linker – sfCherry $3C_{11}$ – IRES – sfCherry $3C_{1-10}$)[28]. Firstly, DNA fragments of wildtype or codon mutant PYCARD sequence and linker sequence (GSGSG), and split sfCherry $3C_{11}$ were synthesized by Twist Bioscience and IDT (Integrated DNA Technologies), respectively. And DNA fragment of sfCherry $3C_{1-10}$ was amplified from the plasmid that was kindly supplied by Dr. Bo Huang at UCSF. Then, the DNA fragments were ligated to the linearized BdLV vector (*Afe*I/*Xba*I) that includes eGFP- CMV promoter-hPGK promoter with NEBuilder® HiFi DNA Assembly Master Mix (New England Biolabs). For both wildtype and codon mutant PYCARD fluorescence reporters, three plasmids were randomly selected for downstream experiment as biological replicates. DNA sequences of the fluorescence reporters in the plasmids were confirmed with Sanger Sequencing (Quintara Biosciences).

To generate cells containing wildtype and codon mutant PYCARD fluorescence reporters, we first produced lentivirus by transfection of confirmed plasmids and pCMV-dR8.91 and pMD2.D plasmids into HEK 293T cells using TransIT-Lenti (Mirus). Virus containing supernatants were harvested 48 h after transfection by passing through a 0.45 μm filter, and were transduced into MDA-MB-231 control and tRNA$^{Ile}_{GAU}$ depletion tRNA$^{Ile}_{UAU}$ overexpression cells using polybrene (Millipore). The transduced cells were cultured for two weeks before flow cytometry analysis.

Fluorescence intensities of mCherry and eGFP in each cell were measured with a FACSCelesta instrument (BD Biosciences) at UCSF. mCherry was excited by 561 nm laser and was detected through 610/20 nm emission filter; GFP was excited by 488 nm laser and was detected through 530/30 nm emission filter. Flow cytometry data was first analyzed

with FlowJo and R. The relative mCherry expression level of each cell was calculated as the fluorescence intensity ratio of mCherry to GFP.

RSCU and Pathway Enrichment Analyses

Gene filtering: The Homo sapiens GRCh38 CDS sequences were downloaded from the Ensembl database. To avoid multiple splice variants from the same gene affecting downstream analysis, principle splice isoforms were filtered using annotations from the APPRIS database and a custom Python script. For genes with multiple annotated isoforms, the transcript with the highest score was chosen as the representative.

RSCU calculation: To calculate the relative synonymous codon usage (RSCU) for a given codon in each gene, we first calculated the total abundances of each codon across our entire filtered CDS dataset to determine the empiric distribution of synonymous codon usage for each amino acid. For each gene, the RSCU score was calculated as: [Observed_Codon_Usage – Expected_Codon_Usage] / Expected_codon_usage. The expected codon usage was defined as Observed_Amino_Acid_Usage * Pr(Codon_Usage | Amino_Acid) where the probability mass function was determined using the empiric codon distribution described above. For genes/transcripts in which a given amino acid appeared zero times, the RSCU score was set to 0.

Mutual Information/Pathway Enrichment: Genes were ranked by the RSCU score calculated above. Mutual information analyses to detect significantly over-represented and under-represented pathways in discrete bins were performed using the iPAGE mutual information framework with pathway annotations built from the Reactome database[29]. Heatmaps were generated with iPAGE. To determine pathways that were most likely to be divergently modulated by AUA or AUC over/under-expression, we additionally filtered the output to include pathway enrichments/depletions present in both AUC and AUA analyses with p-values less than 10E-3 in the highest RSCU bin. Heatmaps were generated using Python software and the seaborn package.

Databases/Sites/Software used: Ensembl: https://useast.ensembl.org/index.html

APPRIS: http://appris-tools.org/#/

iPAGE: https://tavazoielab.c2b2.columbia.edu/iPAGE/

Reactome: https://reactome.org

Python 3.6.0: https://www.python.org

Pandas: https://pandas.pydata.org

Seaborn: https://seaborn.pydata.org

Statistical analysis

Results are presented in dot-plot with dots representing individual values and bar-charts depicting average values with standard error of the mean (±s.e.m.). The number of samples

for each group was chosen based on the expected levels of variation and consistency. FISH quantification was performed in a blinded fashion. Unless otherwise stated, statistical significance was assessed by a two-tailed Student's t-test with P-value < 0.05 being considered statistically significant.

Supplementary Material

Refer to Web version on PubMed Central for supplementary material.

Acknowledgements

Data availability

Experimental data will be available from the corresponding author upon request. Sequencing data will be made available in public databases.

References

1. Ogle JM, Carter AP & Ramakrishnan V Insights into the decoding mechanism from recent ribosome structures. Trends Biochem Sci 28, 259–266, doi:10.1016/S0968-0004(03)00066-5 (2003). [PubMed: 12765838]

2. Schmeing TM & Ramakrishnan V What recent ribosome structures have revealed about the mechanism of translation. Nature 461, 1234–1242, doi:10.1038/nature08403 (2009). [PubMed: 19838167]

3. Pavon-Eternod M et al. tRNA over-expression in breast cancer and functional consequences. Nucleic Acids Res 37, 7268–7280, doi:10.1093/nar/gkp787 (2009). [PubMed: 19783824]

4. Goodarzi H et al. Modulated Expression of Specific tRNAs Drives Gene Expression and Cancer Progression. Cell 165, 1416–1427, doi:10.1016/j.cell.2016.05.046 (2016). [PubMed: 27259150]

5. Gingold H et al. A dual program for translation regulation in cellular proliferation and differentiation. Cell 158, 1281–1292, doi:10.1016/j.cell.2014.08.011 (2014). [PubMed: 25215487]

6. Pavon-Eternod M, Gomes S, Rosner MR & Pan T Overexpression of initiator methionine tRNA leads to global reprogramming of tRNA expression and increased proliferation in human epithelial cells. RNA 19, 461–466, doi:10.1261/rna.037507.112 (2013). [PubMed: 23431330]

7. Vo MN et al. ANKRD16 prevents neuron loss caused by an editing-defective tRNA synthetase. Nature 557, 510–515, doi:10.1038/s41586-018-0137-8 (2018). [PubMed: 29769718]

8. Knott SRV et al. Asparagine bioavailability governs metastasis in a model of breast cancer. Nature 554, 378–381, doi:10.1038/nature25465 (2018). [PubMed: 29414946]

9. Loayza-Puch F et al. Tumour-specific proline vulnerability uncovered by differential ribosome codon reading. Nature 530, 490–494, doi:10.1038/nature16982 (2016). [PubMed: 26878238]

10. Minn AJ et al. Genes that mediate breast cancer metastasis to lung. Nature 436, 518–524, doi:10.1038/nature03799 (2005). [PubMed: 16049480]

11. Goodarzi H, Elemento O & Tavazoie S Revealing global regulatory perturbations across human cancers. Mol Cell 36, 900–911, doi:10.1016/j.molcel.2009.11.016 (2009). [PubMed: 20005852]

12. McGlincy NJ & Ingolia NT Transcriptome-wide measurement of translation by ribosome profiling. Methods 126, 112–129, doi:10.1016/j.ymeth.2017.05.028 (2017). [PubMed: 28579404]

13. Gill JG, Piskounova E & Morrison SJ Cancer, Oxidative Stress, and Metastasis. Cold Spring Harb Symp Quant Biol 81, 163–175, doi:10.1101/sqb.2016.81.030791 (2016). [PubMed: 28082378]

14. Loo JM et al. Extracellular metabolic energetics can promote cancer progression. Cell 160, 393–406, doi:10.1016/j.cell.2014.12.018 (2015). [PubMed: 25601461]

15. Nguyen A, Yoshida M, Goodarzi H & Tavazoie SF Highly variable cancer subpopulations that exhibit enhanced transcriptome variability and metastatic fitness. Nat Commun 7, 11246, doi:10.1038/ncomms11246 (2016). [PubMed: 27138336]

16. Piskounova E et al. Oxidative stress inhibits distant metastasis by human melanoma cells. Nature 527, 186–191, doi:10.1038/nature15726 (2015). [PubMed: 26466563]

17. Katibah GE et al. Broad and adaptable RNA structure recognition by the human interferon-induced tetratricopeptide repeat protein IFIT5. Proc Natl Acad Sci U S A 111, 12025–12030, doi:10.1073/pnas.1412842111 (2014). [PubMed: 25092312]

18. Mohr S et al. Thermostable group II intron reverse transcriptase fusion proteins and their use in cDNA synthesis and next-generation RNA sequencing. RNA 19, 958–970, doi:10.1261/rna.039743.113 (2013). [PubMed: 23697550]

19. Goodarzi H RiboLog, <github.com/Goodarzilab/Ribolog> (2019).

20. Nguyen A et al. PKLR promotes colorectal cancer liver colonization through induction of glutathione synthesis. J Clin Invest 126, 681–694, doi:10.1172/JCI83587 (2016). [PubMed: 26784545]

21. Chaudhuri AD, Yelamanchili SV & Fox HS Combined fluorescent in situ hybridization for detection of microRNAs and immunofluorescent labeling for cell-type markers. Front Cell Neurosci 7, 160, doi:10.3389/fncel.2013.00160 (2013). [PubMed: 24065888]

22. Stewart SA et al. Lentivirus-delivered stable gene silencing by RNAi in primary cells. RNA 9, 493–501 (2003). [PubMed: 12649500]

23. Bryant DM et al. A molecular network for de novo generation of the apical surface and lumen. Nat Cell Biol 12, 1035–1045, doi:10.1038/ncb2106 (2010). [PubMed: 20890297]

24. Chen B et al. Dynamic imaging of genomic loci in living human cells by an optimized CRISPR/Cas system. Cell 155, 1479–1491, doi:10.1016/j.cell.2013.12.001 (2013). [PubMed: 24360272]

25. Yeo NC et al. An enhanced CRISPR repressor for targeted mammalian gene regulation. Nat Methods 15, 611–616, doi:10.1038/s41592-018-0048-5 (2018). [PubMed: 30013045]

26. Xiao Z, Zou Q, Liu Y & Yang X Genome-wide assessment of differential translations with ribosome profiling data. Nat Commun 7, 11194, doi:10.1038/ncomms11194 (2016). [PubMed: 27041671]

27. Gandin V et al. nanoCAGE reveals 5' UTR features that define specific modes of translation of functionally related MTOR-sensitive mRNAs. Genome Res 26, 636–648, doi:10.1101/gr.197566.115 (2016). [PubMed: 26984228]

28. Feng S et al. Bright split red fluorescent proteins for the visualization of endogenous proteins and synapses. Commun Biol 2, 344, doi:10.1038/s42003-019-0589-x (2019). [PubMed: 31552297]

29. Goodarzi H, Hottes AK & Tavazoie S Global discovery of adaptive mutations. Nat Methods 6, 581–583, doi:10.1038/nmeth.1352 (2009). [PubMed: 19597501]
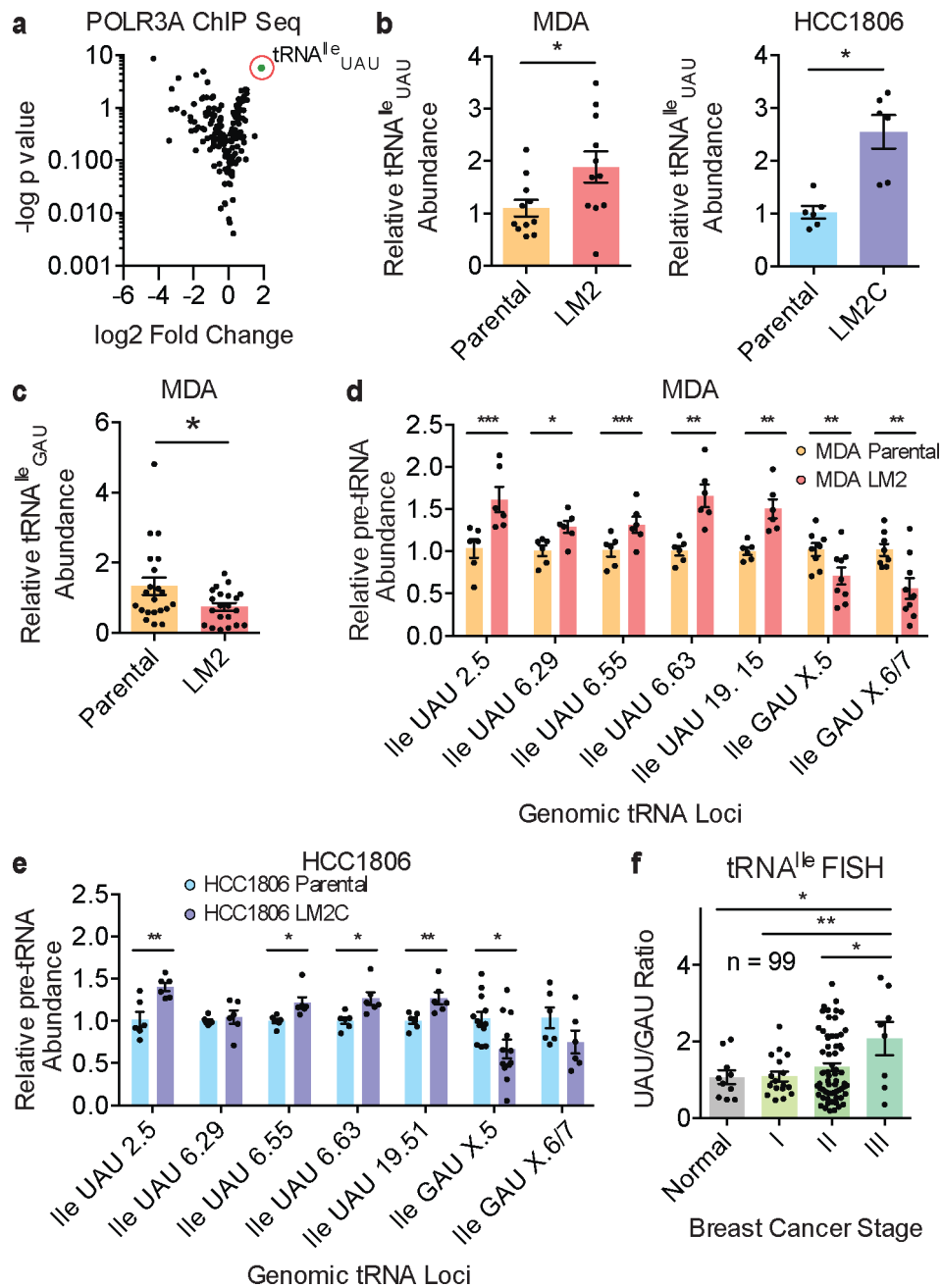
Figure 1 –. Isoleucine isoacceptors are differentially modulated in isogenic poorly and highly metastatic breast cancer pairs.

(a) Volcano plot representing log2 fold change vs. −log p value of POL3RA ChIP sequencing analysis of MDA-LM2 cells vs. MDA-MB-231 Parental cells.

(b) tRNA$^{Ile}_{UAU}$ quantification by specific tRNA$^{Ile}_{UAU}$ probe RT-qPCR normalized to 18S probes of highly metastatic LM2 lines relative to their parental MDA-MB-231 and HCC1806 cell lines.

(c) tRNA$^{Ile}_{GAU}$ quantification by specific tRNA$^{Ile}_{GAU}$ probe RT-qPCR normalized to 18S probes of highly metastatic LM2 lines relative to the parental MDA-MB-231 cell line.

(d,e) Relative pre-tRNA abundance of tRNA$^{Ile}_{UAU}$ and tRNA$^{Ile}_{GAU}$ across multiple primers covering distinct genetic loci using RT-qPCR of MDA-LM2 vs. MDA-MB-231 (d) & HCC1806-LM2C vs. HCC1806 Parental cells (e).
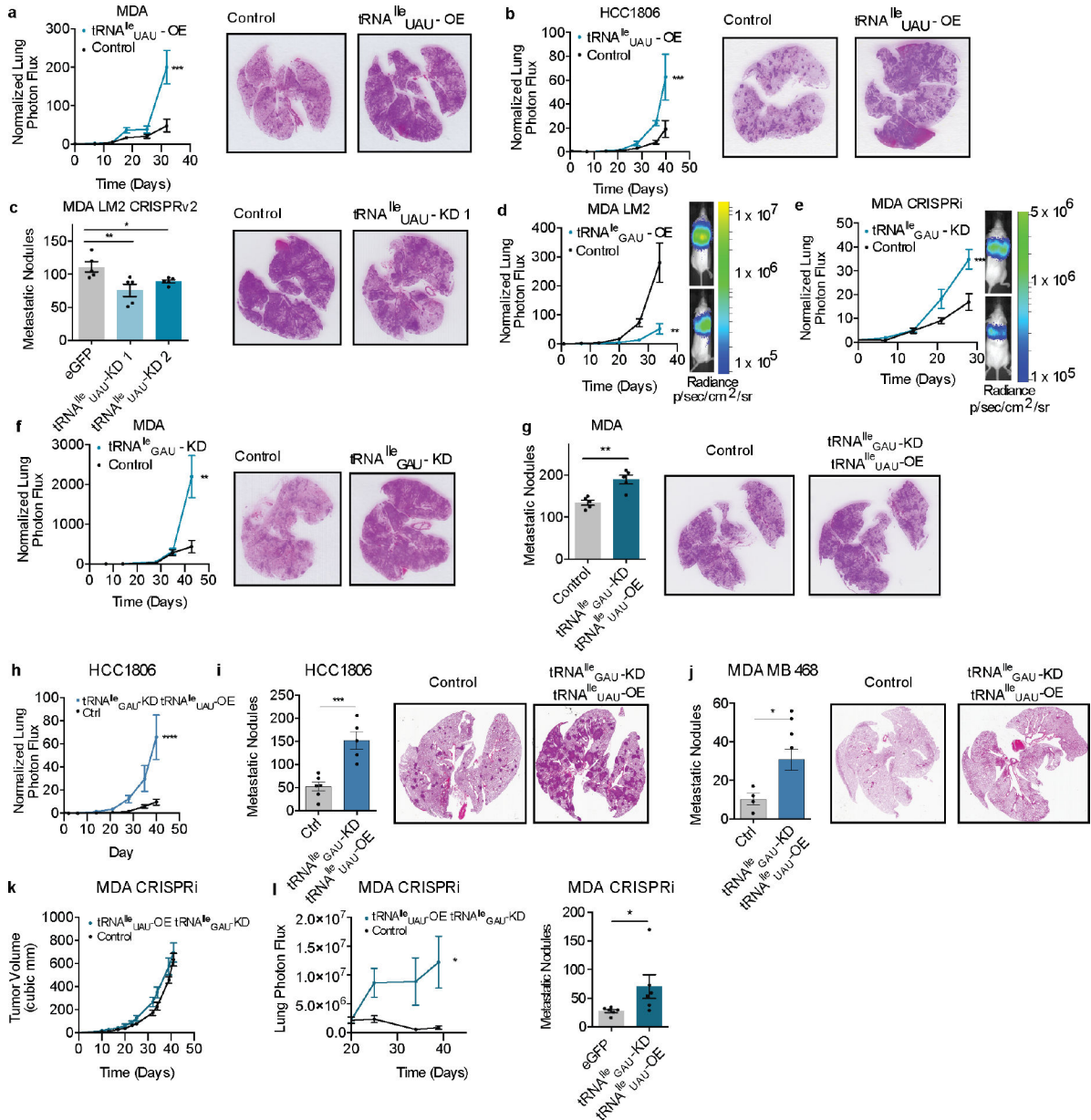
(f) Relative tRNA$^{Ile}_{UAU}$/tRNA$^{Ile}_{GAU}$ ratios quantified by fluorescent intensity normalized to DAPI of breast tissue microarrays, stratified by normal tissue or breast cancer stage I & II, III, measured by FISH with LNA targeting tRNA$^{Ile}_{UAU}$ or tRNA$^{Ile}_{GAU}$. Two-sided un-paired student's t-tests performed, p-values $p<0.05$, $p<0.01$, $p<0.001$ represented as *, **, ***, respectively.

Figure 2 –. tRNAIleUAU promotes & tRNAIleGAU suppresses metastatic colonization.

(a-b) Bioluminescent imaging post tail vein injection of 1×10^5 of MDA Parental (a) or 1.5×10^5 HCC1806 (b) cells overexpressing tRNA$^{Ile}_{UAU}$ or control with representative lung histology stained with H&E; n=5 in each cohort.

(c) Quantification of lung metastatic nodules post extraction after tail vein injection of 5×10^4 LM2 CRISPR cells guides targeting eGFP or tRNA$^{Ile}_{UAU}$, with representative histology for control & tRNA$^{Ile}_{UAU}$ guide 1; n=5 in each cohort.

(d) Bioluminescence imaging after tail vein injection of 1×10^5 of MDA LM2 cells overexpressing tRNA$^{Ile}_{GAU}$ or control with representative images; luminescence expressed as Radiance p/sec/cm^2/sr; n=5 in each cohort.

(e,f) Same as (d) with MDA Parental CRISPRi cells with guides targeting either control or tRNA$^{Ile}_{GAU}$ (e) or shRNA targeting control or tRNA$^{Ile}_{GAU}$ with representing H&E lung histology (f).

(g) Quantification of lung metastatic nodules post extraction after tail vein injection of 5.0×10^4 MDA cells with CRISPRi targeting tRNA$^{Ile}_{GAU}$ and tRNA$^{Ile}_{UAU}$ overexpression or control; n=5–6 in each cohort, with representative histology for control & tRNA$^{Ile}_{GAU}$ depletion and tRNA$^{Ile}_{UAU}$ overexpression.

(h) Bioluminescent imaging post tail vein injection of 1.5×10^5 HCC1806 cells with shRNA targeting tRNA$^{Ile}_{GAU}$ and tRNA$^{Ile}_{UAU}$ overexpression or control; n=5–6 in each cohort.

(i) Quantification of lung metastatic nodules post extraction after tail vein injection described in (a) with representative histology for control & tRNA$^{Ile}_{GAU}$ depletion and tRNA$^{Ile}_{UAU}$ overexpression.

(j) Quantification of lung metastatic nodules post extraction after tail vein injection of 1×10^6 of MDA MB 468 cells shRNA targeting tRNA$^{Ile}_{GAU}$ and tRNA$^{Ile}_{UAU}$ overexpression or control with representative images, n=5 in each cohort.

(k) Primary tumor growth curves of NSG mice injected with either 1×10^6 MDA MB 231 control or tRNA$^{Ile}_{GAU}$ depletion tRNA$^{Ile}_{UAU}$ overexpression cells in mammary fat pad with 1:1 Matrigel, volume measured in cubic mm, n=6 mice.

(l) Bioluminescent imaging of lungs and quantification of lung metastatic nodules post extraction from orthotopic mammary fat pad injections described in (k). Statistics utilized include 2-way ANOVA for imaging and two-sided unpaired student's t-test for nodule quantification, p-values p<0.05, p<0.01, p<0.001 represented as *, **, ***, respectively.
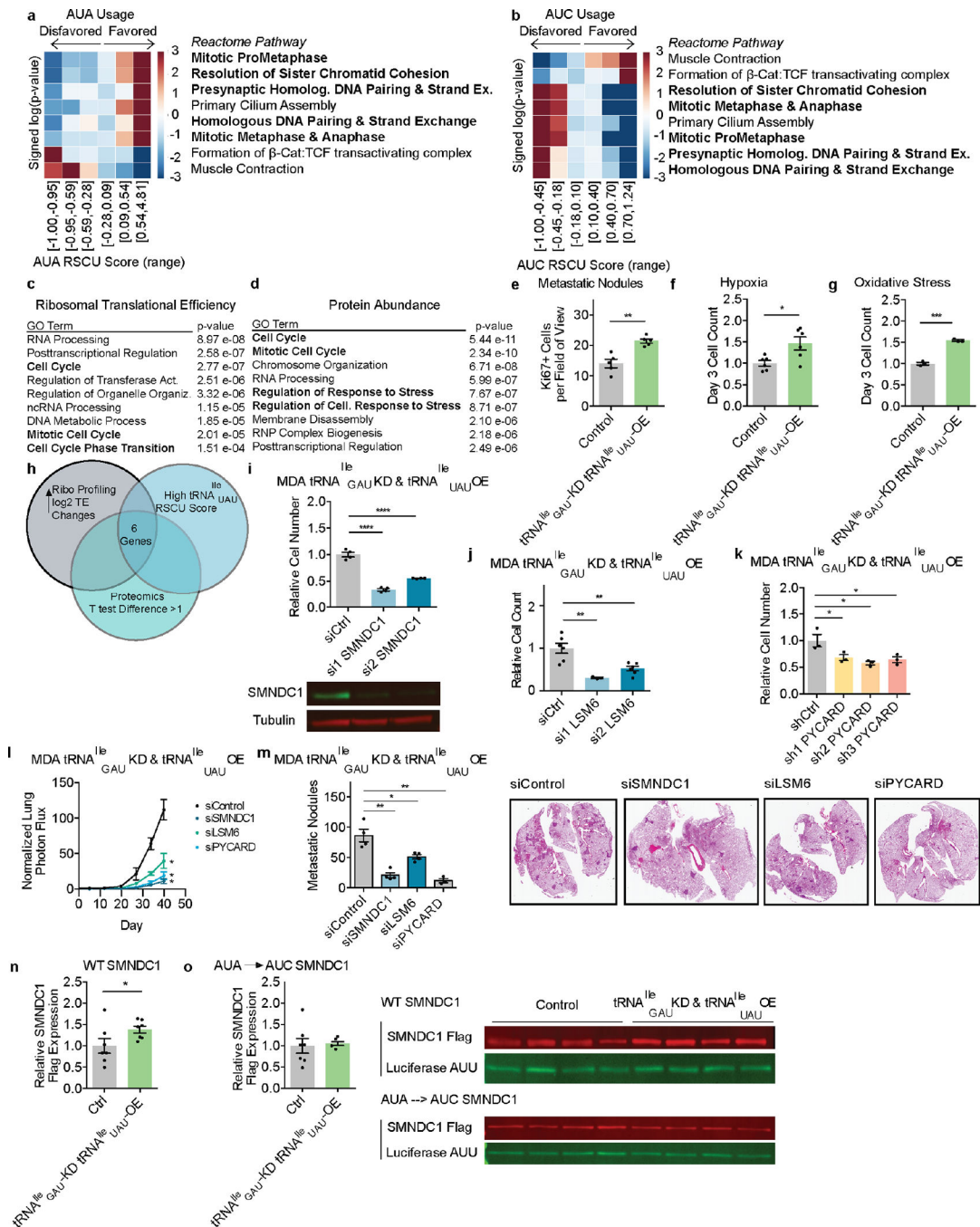
Figure 3 - Cell Cycle and Response to Stress gene expression and phenotypes characterize tRNA$^{\text{Ile}}$ modulations.

(a,b) Reactome pathways significantly enriched in AUA (a) or AUC (b) by relative synonymous codon usage (RSCU) using iPAGE.

(c,d) GO function terms for positive and significant TE changes from ribosomal profiling (c) or label free quantification by mass spectrometry (d) in tRNA$^{\text{Ile}}_{\text{GAU}}$ depletion and tRNA$^{\text{Ile}}_{\text{UAU}}$ overexpression cells versus control.

(e) Quantification of Ki67 immunofluorescence staining in MDA MB 231 tRNA$^{\text{Ile}}_{\text{GAU}}$ depletion and tRNA$^{\text{Ile}}_{\text{UAU}}$ overexpression cells versus control.

(f,g) Relative cell counts of MDA MB 231 control & tRNA$^{Ile}_{GAU}$ depletion tRNA$^{Ile}_{UAU}$ overexpression cells exposed to 0.5% hypoxia (f) or treated with 200uM H$_2$0$_2$ (g) for 3 days.

(h) Venn Diagram of overlapping datasets to identify downstream effectors – includes high RSCU tRNA$^{Ile}_{UAU}$ score (top 50%), and genes with significantly positive changes in TE and proteomics in both MDA LM2 vs. MDA Parental cells and tRNA$^{Ile}_{GAU}$ depletion tRNA$^{Ile}_{UAU}$ overexpression cells vs. control.

(i) Relative cell count of MDA tRNA$^{Ile}_{GAU}$ depletion tRNA$^{Ile}_{UAU}$ overexpression cells treated with control or SMNDC1 siRNA in 0.5% hypoxia for 2 days. Western performed on siRNA cells on day 3.

(j) Relative cell counts of MDA tRNA$^{Ile}_{GAU}$ depletion tRNA$^{Ile}_{UAU}$ overexpression cells treated with control or LSM6 siRNA for 3 days.

(k) Relative cell counts of MDA tRNA$^{Ile}_{GAU}$ depletion tRNA$^{Ile}_{UAU}$ overexpression cells transduced with shRNA targeting either control or PYCARD for 3 days.

(l) Bioluminescent imaging of lungs of NSG mice injected with 1×10^6 MDA tRNA$^{Ile}_{GAU}$ depletion tRNA$^{Ile}_{UAU}$ overexpression cells with either siRNA targeting SMNDC1, LSM6, PYCARD, or control, n=3–5 mice per group.

(m) Quantification and H&E histology of lung metastatic nodules post extraction after tail vein injections described in (l).

(n,o) LICOR Western quantification of either Flag tagged wildtype (n) or all AUA to AUC codons (n) SMNDC1 expression relative to reporter control luciferase (all Ile AUU) 24 hours post transfection in either MDA control or tRNA$^{Ile}_{GAU}$ depletion tRNA$^{Ile}_{UAU}$ overexpression cells. Representative images below. Statistics utilized include 2-way ANOVA for imaging and two-sided un-paired student's's t-tests performed, p-values *, **, **** indicated as p<0.05, p<0.01, and p<0.0001, respectively.
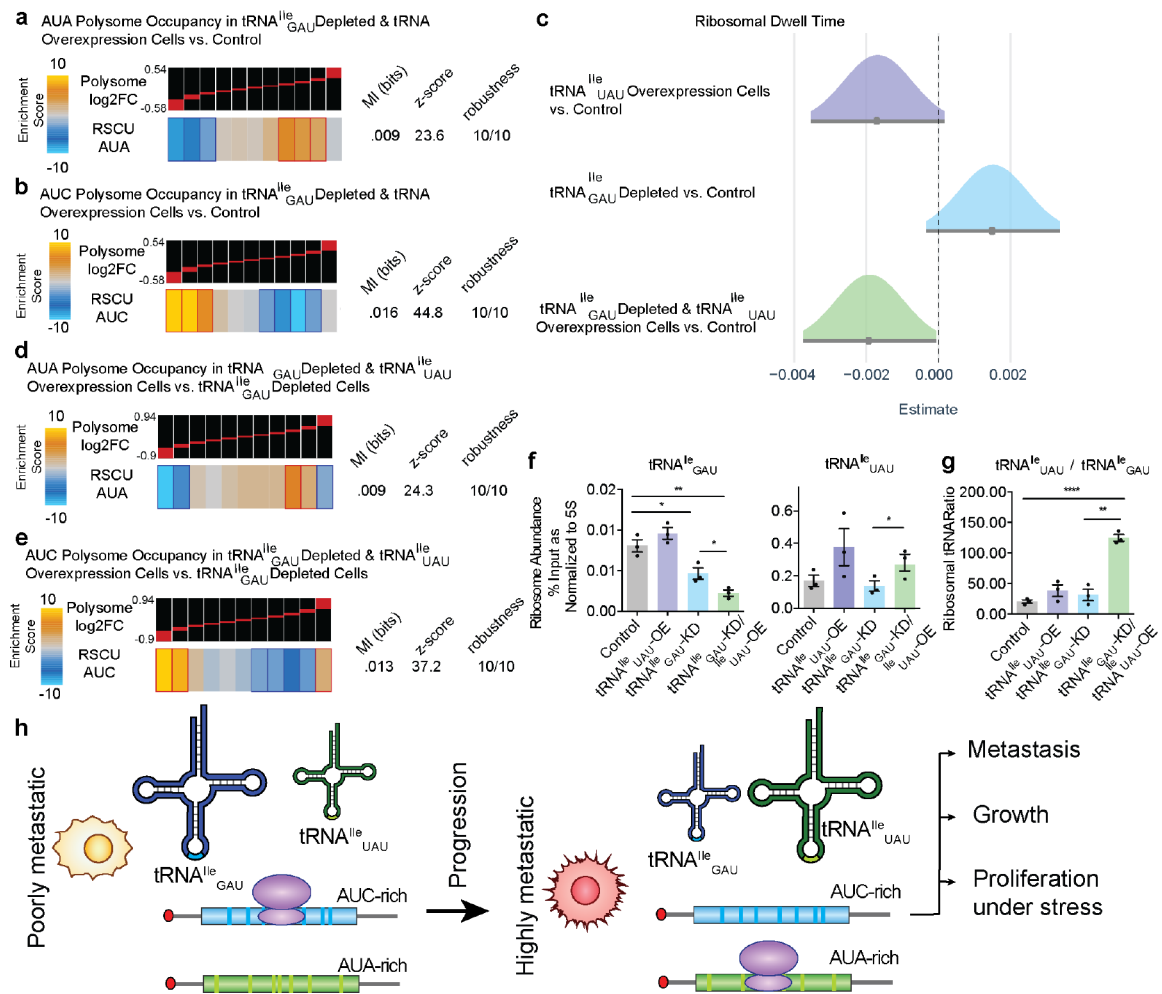
Figure 4 –. Translational efficiency of AUA enriched transcripts is dependent on tRNA$^{Ile}_{GAU}$ abundance.

(a) Genes with a high abundance of AUA codons (using RSCU scores) were significantly enriched among genes upregulated in polysomes (corrected for their transcript changes) in tRNA$^{Ile}_{GAU}$ depleted tRNA$^{Ile}_{UAU}$ overexpression cells versus control MDA-MB-231 cells. The statistical significance of these enrichments was assessed using mutual-information calculations and associated Z score (based on randomized input vectors) and robustness scores (based on jackknifing tests). The heatmap was generated using the −log of the hypergeometric p-value for enrichment and log of p-value for depletion (collectively termed the enrichment score). The red and dark-blue borders indicate the statistical significance of the calculated hypergeometric p-values (for details, see Goodarzi et al., 2009)[11].

(b) Same as (a) except analyzed for AUC codon enrichment, showing significantly depletion among genes upregulated in polysomes (corrected for their transcript changes) in tRNA$^{Ile}_{GAU}$ depleted tRNA$^{Ile}_{UAU}$ overexpression cells versus control MDA-MB-231 cells.

(c) Ribosomal AUA codon dwelling times as estimated by CELP bias coefficients (higher bias coefficient indicates longer dwelling time). Univariate regression coefficients estimating the effects of tRNA^{Ile} modulated MDA cells. A 95% confidence interval excluding zero

(not overlapping the vertical line x=0) means that the tested effect was significant at α=0.05 (p<0.05).

(d) Hypergeometric distribution shown as a z- score of AUA codon enrichment of polysome transcripts represented as log2 fold change of $\text{tRNA}^{\text{Ile}}_{\text{GAU}}$ depleted $\text{tRNA}^{\text{Ile}}_{\text{UAU}}$ overexpression cells versus $\text{tRNA}^{\text{Ile}}_{\text{GAU}}$ depleted MDA MB 231 cells, stratified in bins of 10, increased log2 fold change from left to right. AUA codon representation visualized as a value ranging from −10 to 10 relative to the average.

(e) Same as (d) except analyzed for AUC codon enrichment.

(f) Ribosome abundance of tRNA^{Ile} quantified by specific $\text{tRNA}^{\text{Ile}}_{\text{GAU}}$ (left) and $\text{tRNA}^{\text{Ile}}_{\text{UAU}}$ (right) probes. RT-qPCR normalized to 5S probes of tRNA^{Ile} modulated MDA cells from polysome fractions, measured as % Input.

(g) Ribosomal ratio of $\text{tRNA}^{\text{Ile}}_{\text{UAU}}$/ $\text{tRNA}^{\text{Ile}}_{\text{GAU}}$ abundance quantified by specific $\text{tRNA}^{\text{Ile}}_{\text{GAU}}$ probe and $\text{tRNA}^{\text{Ile}}_{\text{UAU}}$ probe RT-qPCR normalized to 5S probes of tRNA^{Ile} modulated MDA cells from polysome fractions, measured as % Input.

(h) Model depicting how tRNA^{Ile} abundance shifts alter translational dynamics and metastatic phenotypes. Two-sided un-paired student's's t-tests performed, p-values represented as *, ** as p<0.05, p<0.01 respectively.